

Supporting Information

Growth of BiVO₄ Nanoparticles on WO₃ Porous Scaffold: Improved Water-Splitting by High Band-Edge Light Harvesting

Kiwon Kim^a, Sung Kyung Nam, Jong Hyeok Park^b and Jun Hyuk Moon^{,a}*

^aDepartment of Chemical and Biomolecular Engineering, Sogang University

35 Baekbum-ro Mapo-gu, Seoul, 04107, Republic of Korea

^bDepartment of Chemical and Biomolecular Engineering, Yonsei University

50 Yonsei-ro Seodaemun-gu, Seoul, 03722, Republic of Korea

*Corresponding author, E-mail: junhyuk@sogang.ac.kr

Table S1. Water oxidation photocurrent density and onset potential of various WO₃/BiVO₄ photoanodes.

Electrode	J _{H₂O} at 1.23V _{RHE} [mA/cm ²]	IPCE (%) at 500nm	Reference
WO ₃ /BiVO ₄ IO	1.3*	5	1
WO ₃ /BiVO ₄ porous structure	4.7*	3	2
WO ₃ /W:BiVO ₄ /BiVO ₄	2.6	-	3
WO ₃ /BiVO ₄ IO	5.1*	5	4
WO ₃ /W:BiVO ₄ NRs	3.1	6	5
WO ₃ /(W,Mo)-BiVO ₄ Nanohelix	5.3*	8	6
WO ₃ /BiVO ₄ NRs	3.25*	5	7
WO ₃ /M:BiVO ₄ film	1.7	5	8
WO ₃ /SnO ₂ /BiVO ₄ film	2.5	3	9
SnO ₂ /WO ₃ /BiVO ₄ film	1.8	2	10
WO ₃ /BiVO ₄ film	1.5	7.5	11
BiVO ₄ /WO ₃ NRs	1.2	2	12

* The value in parentheses is the water splitting current of the electrode coated with the oxygen evolution catalyst.

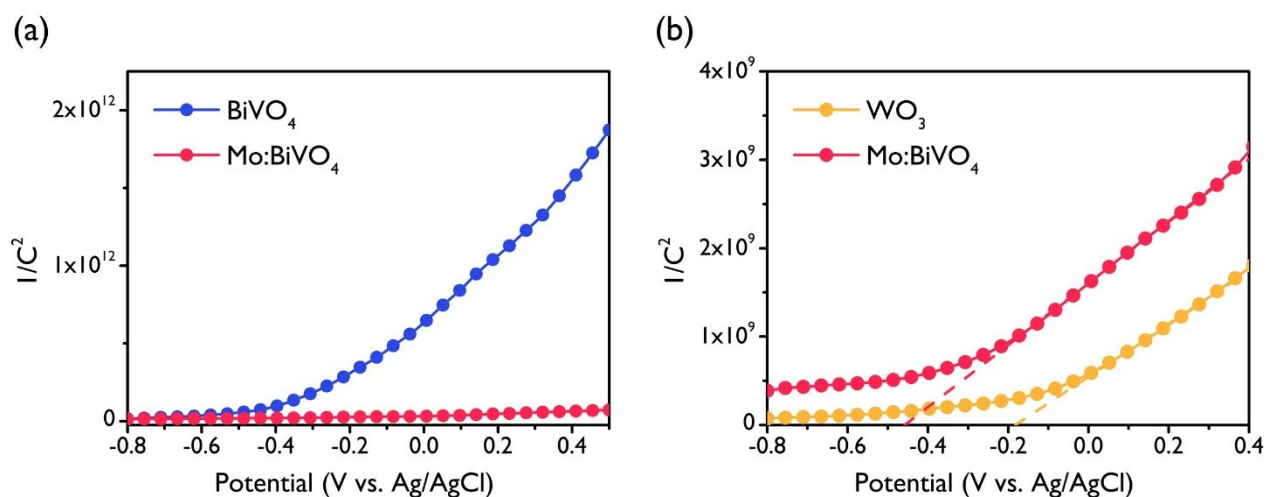


Figure S1. (a) Mott-Schottky plots of WO_3 and BiVO_4 films. (b) Mott-Schottky plots of BiVO_4 before and after Mo doping. Mott-Schottky measurements were conducted using impedance spectroscopy in a dark environment in 0.5 M Na_2SO_4 solution at a frequency of 1 kHz. We compared the carrier densities before and after doping, $2.33 \times 10^{21} \text{ cm}^{-3}$ for Mo-doped BiVO_4 and $7.33 \times 10^{19} \text{ cm}^{-3}$ for pristine BiVO_4

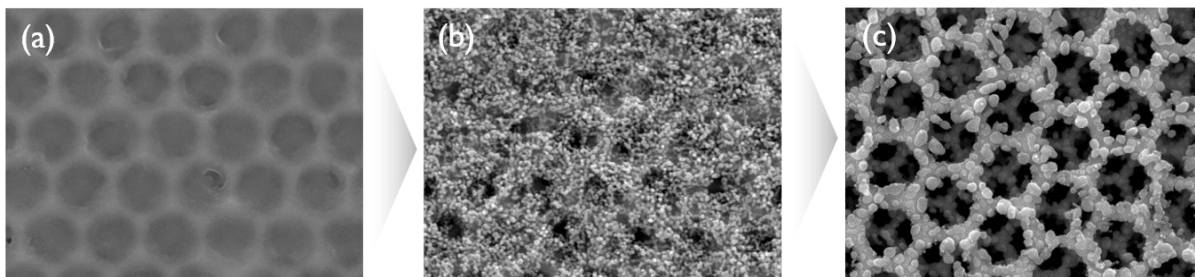


Figure S2. SEM images of WO_3 porous structure with polymer nanosphere-infiltrated BiVO_4 precursor after annealing with different temperature (a) 70 °C, (b) 340 °C and (c) 450 °C.

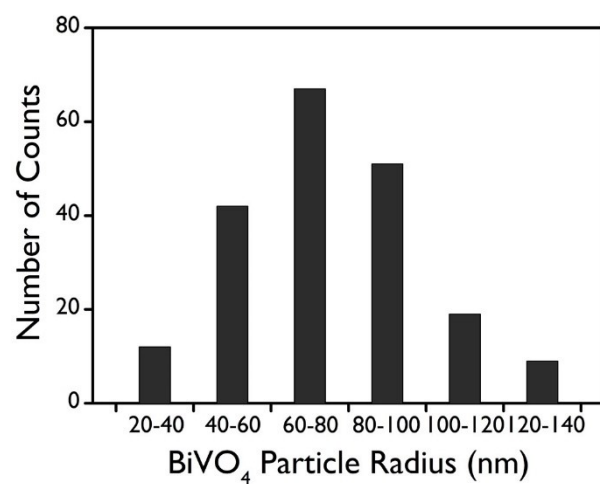


Figure S3. Particle radius distribution of BiVO₄ NP coated on the WO₃ structure. The distribution was obtained from measuring diameters of 200 particles.

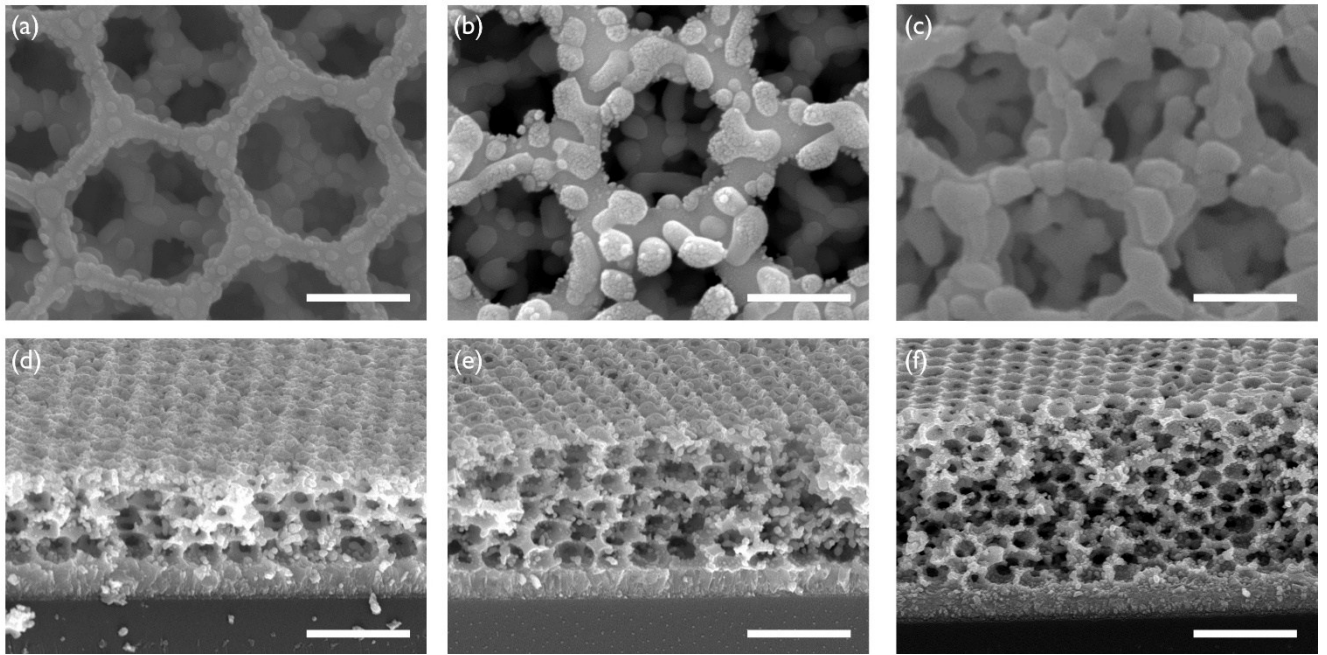


Figure S4. SEM images of BiVO_4 nanoparticles prepared by various precursor concentrations (a-c) and thicknesses (d-f).

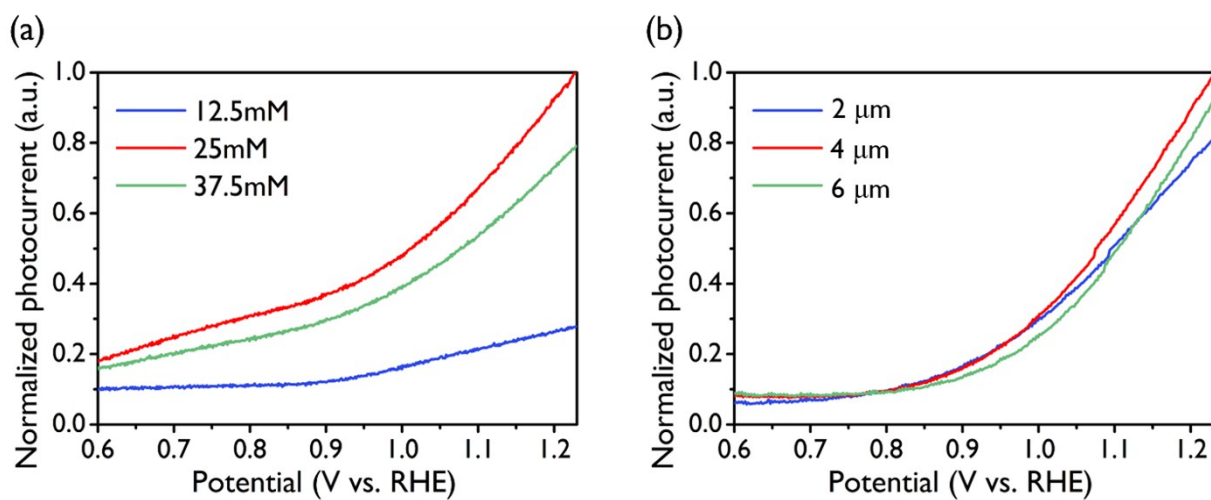


Figure S5. Current-potential (J-V) curves of BiVO₄ NP/WO₃ photoanodes a) with various precursor concentrations of BiVO₄ and b) with various photoanode thicknesses. The coating thickness of BiVO₄ layer was not optimized.

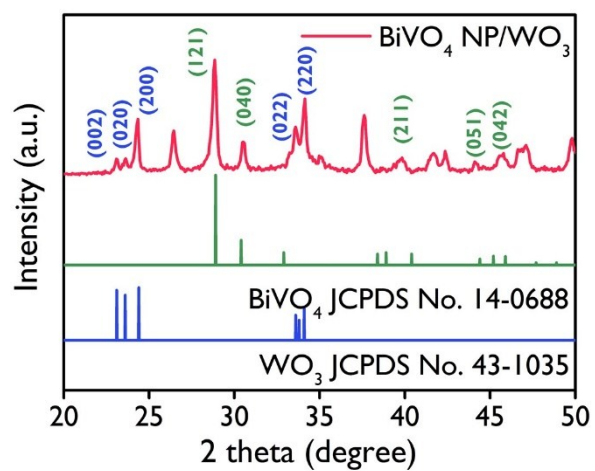


Figure S6. XRD pattern of the Mo:BiVO₄ NP/WO₃. The typical (121) and (040) planes of scheelite-monoclinic BiVO₄ were observed, and the (002), (020), (200) and (220) planes of monoclinic WO₃ were also observed.

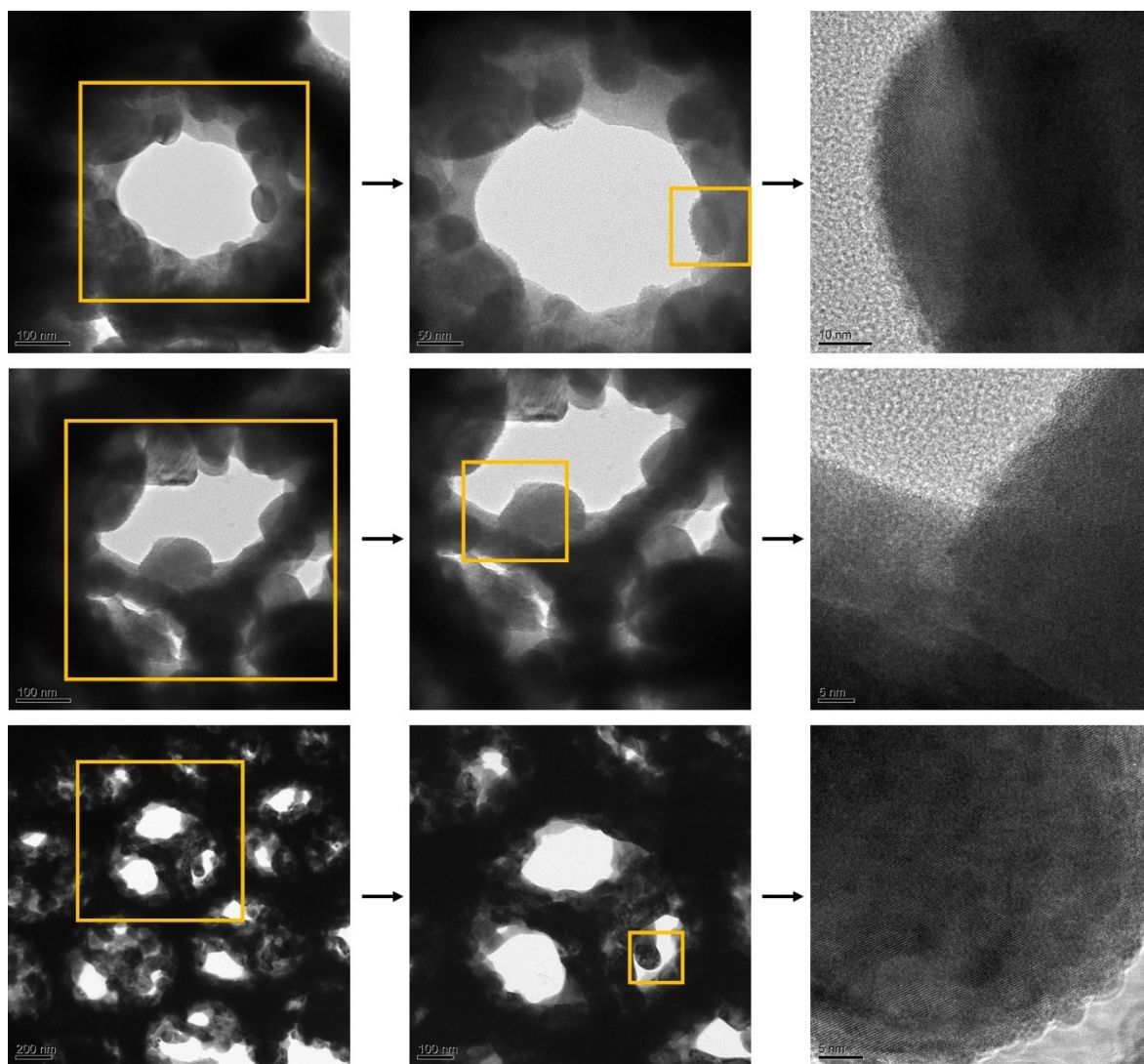


Figure S7. BiVO₄ NP/WO₃ TEM images with various magnifications.

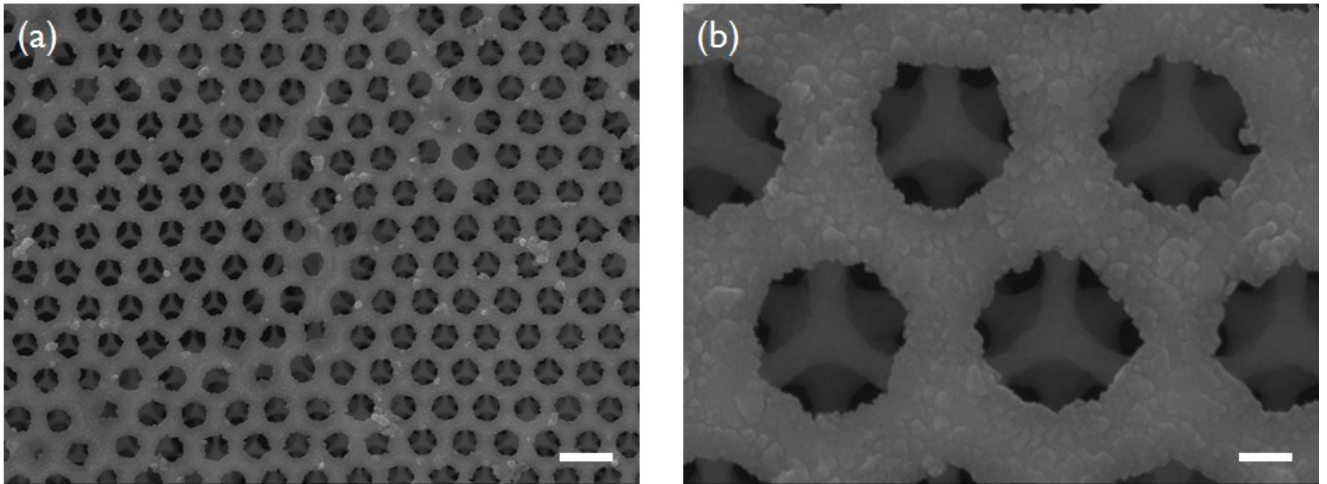


Figure S8. (a) SEM image and (b) high magnification SEM image of BiVO_4 shell / WO_3 photoanode. The scale bars are (a) $1\mu\text{m}$ and (b) $200\mu\text{m}$.

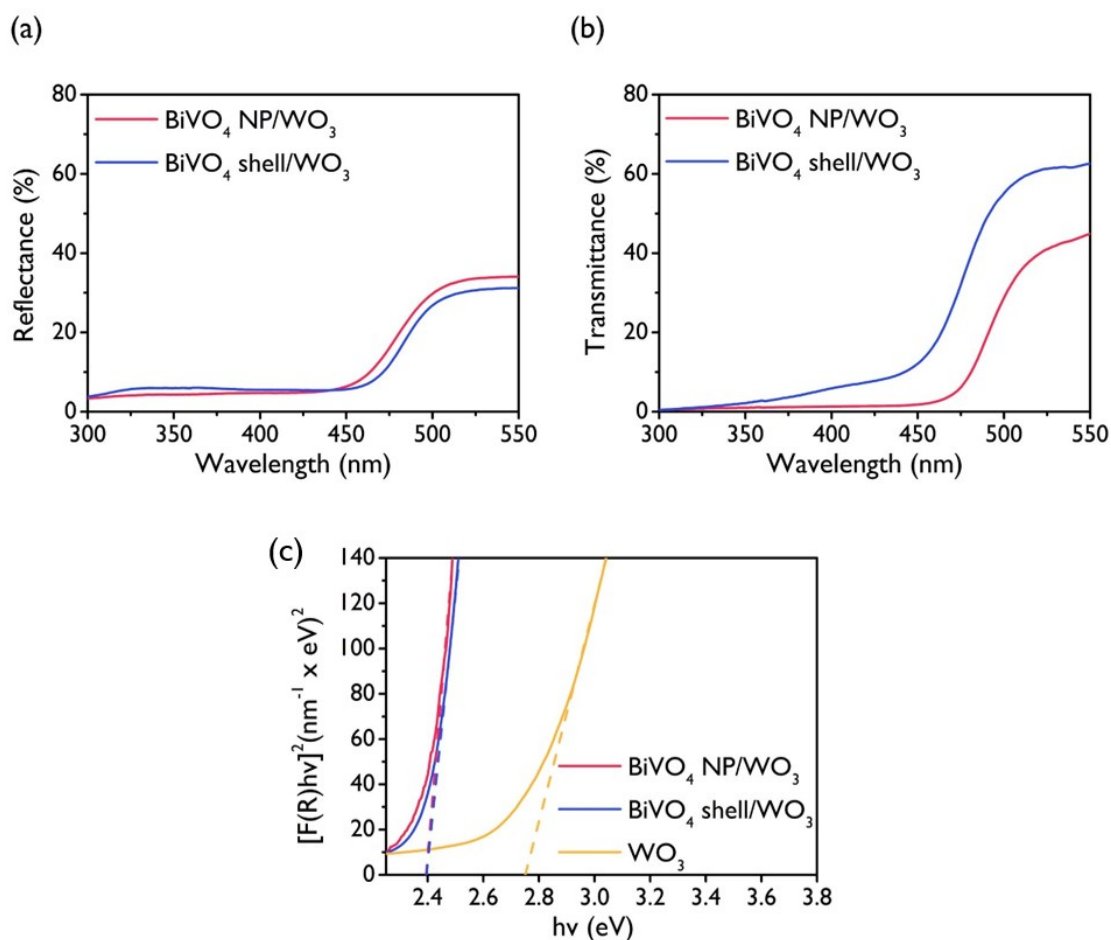


Figure S9. a) Diffuse-reflectance spectra, b) diffuse-transmittance spectra and c) Tauc plots using the Kubelka-Munk function of the BiVO₄ NP/WO₃ and BiVO₄ shell/WO₃ structures. The optical bandgap energy was measured using the Tauc relation, $(ahv)^n = A(hv - E_g)$, where a denotes the absorption coefficient, hv is the photon energy, A is a constant, E_g is the bandgap, and the exponent n depends on the type of transition ($n = 2$ for direct bandgap). The Kubelka-Munk function, $F(R)$, was employed to obtain the absorption coefficient, a ; the Kubelka-Munk equation is $a = (1-R)^2/2R$, where R corresponds to the diffuse reflectance.

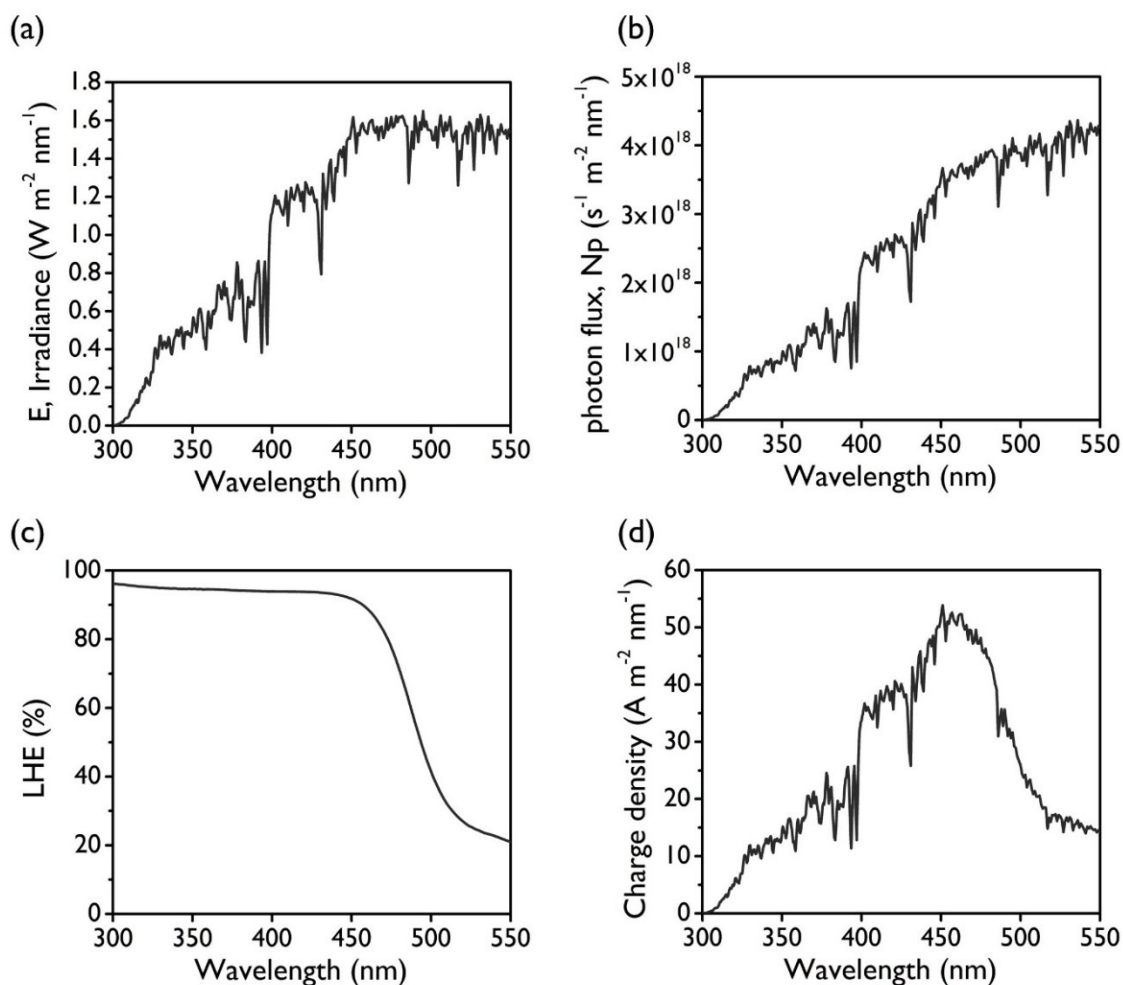


Figure S10. Details of the calculation of the separation efficiency is following.

a) Global tilt spectra irradiance, E.

b) Photon flux, N_p , calculated by the irradiance/energy of a photon: $E/(hc/\lambda) = E \times \lambda \times (5.04 \times 10^{15})$, where h is Plank's constant (4.13×10^{-15} eV s⁻¹), c is the velocity of light (3×10^8 m s⁻¹), and λ is the wavelength.

c) LHE of BiVO₄/WO₃ photoanodes

d) Charge density of BiVO₄/WO₃ photoanodes calculated by $N_p \times e \times \text{LHE}$, where e is the elementary charge (1.6022×10^{-19} C), and $J_{\text{max}} \times \eta_{\text{abs}}$ represents the integration of the charge density.

The product of $J_{\text{max}} \times \eta_{\text{abs}}$ was obtained from the integration of the charge density, which is $N_p \times e \times \text{LHE}$, where N_p is the photon flux of the AM 1.5G spectrum, and e is the elementary charge (1.6022×10^{-19} C).

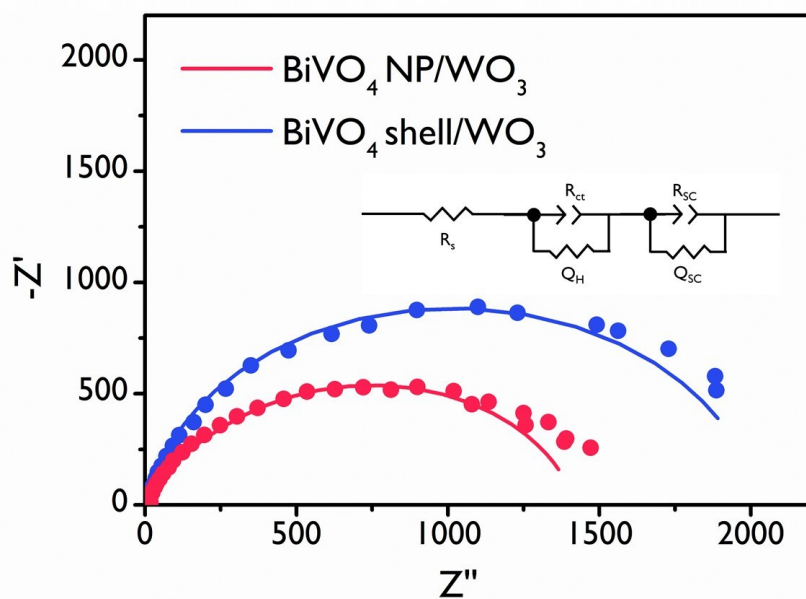


Figure S11. Nyquist plot of BiVO_4 NP/ WO_3 and BiVO_4 shell/ WO_3 . This experiment was also analyzed under 1 sun illumination and at 0.6 V_{RHE} . We compared the charge transfer resistance (R_{ct}) through an equivalent circuit. The resistances of BiVO_4 NP / WO_3 and BiVO_4 shell / WO_3 are 1297 Ω and 1951 Ω , respectively.

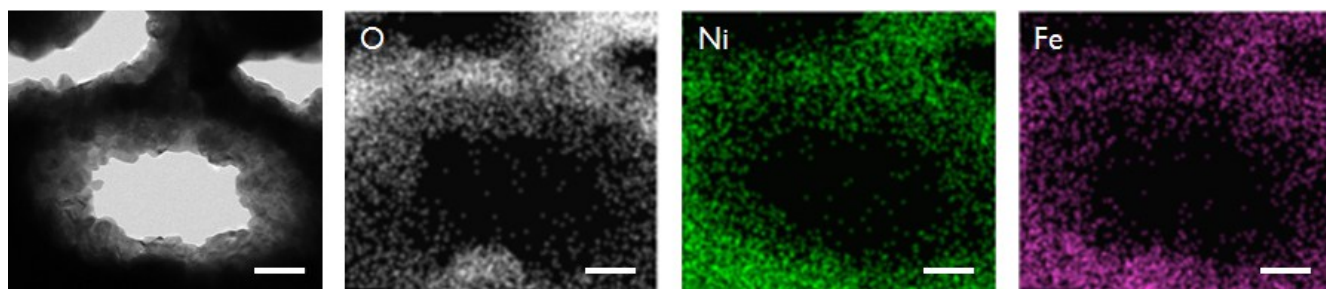


Figure S12. TEM elemental mapping of Fe and Ni for the FeOOH/NiOOH/BiVO₄ NP/WO₃.

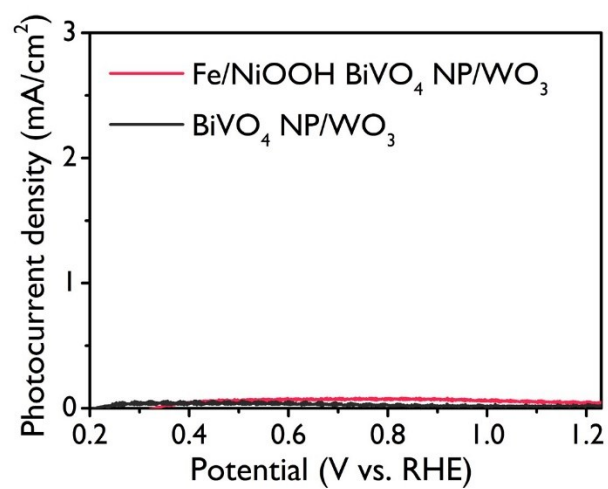


Figure S13. Photocurrent-voltage curves of BiVO₄ NP/WO₃ and FeOOH/NiOOH/BiVO₄ NP/WO₃ photoanodes without illumination.

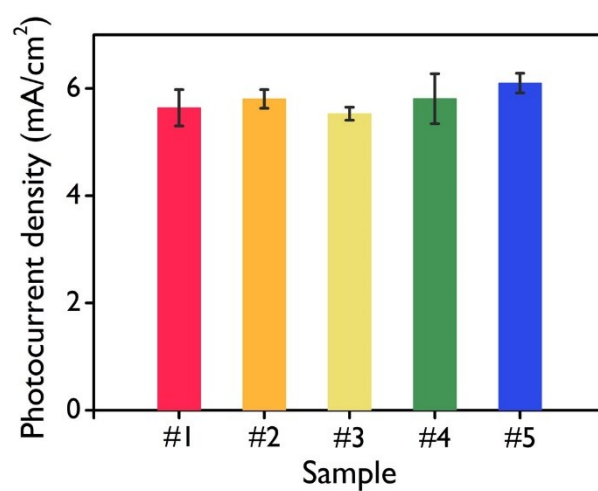


Figure S14. Independent runs of the FeOOH/NiOOH/BiVO₄ NP/WO₃ photoanode at 1.23 V_{RHE} under AM 1.5G illumination.

Reference

1. H. Zhang, W. Zhou, Y. Yang and C. Cheng, *Small*, 2017, **13**, 1603840.
2. S. S. Kalanur, I.-H. Yoo, J. Park and H. Seo, *J. Mater. Chem. A*, 2017, **5**, 1455-1461.
3. J. Choi, P. Sudhagar, J. H. Kim, J. Kwon, J. Kim, C. Terashima, A. Fujishima, T. Song and U. Paik, *Phys. Chem. Chem. Phys.*, 2017, **19**, 4648-4655.
4. M. Ma, X. Shi, K. Zhang, S. Kwon, P. Li, J. K. Kim, T. T. Phu, G.-R. Yi and J. H. Park, *Nanoscale*, 2016, **8**, 3474-3481.
5. P. M. Rao, L. Cai, C. Liu, I. S. Cho, C. H. Lee, J. M. Weisse, P. Yang and X. Zheng, *Nano Lett.*, 2014, **14**, 1099-1105.
6. X. Shi, I. Y. Choi, K. Zhang, J. Kwon, D. Y. Kim, J. K. Lee, S. H. Oh, J. K. Kim and J. H. Park, *Nat. Commun.*, 2014, **5**, 4775.
7. Y. Pihosh, I. Turkevych, K. Mawatari, T. Asai, T. Hisatomi, J. Uemura, M. Tosa, K. Shimamura, J. Kubota and K. Domen, *Small*, 2014, **10**, 3692-3699.
8. K. Zhang, X.-J. Shi, J. K. Kim and J. H. Park, *Phys. Chem. Chem. Phys.*, 2012, **14**, 11119-11124.
9. R. Saito, Y. Miseki and K. Sayama, *Chem. Commun.*, 2012, **48**, 3833-3835.
10. S. n. Murcia-López, C. Fàbrega, D. n. Monllor-Satoca, M. D. Hernández-Alonso, G. n. Penelas-Pérez, A. Morata, J. R. Morante and T. Andreu, *ACS Appl. Mater. Inter.*, 2016, **8**, 4076-4085.
11. S. J. Hong, S. Lee, J. S. Jang and J. S. Lee, *Energy Environ. Sci.*, 2011, **4**, 1781-1787.
12. J. Su, L. Guo, N. Bao and C. A. Grimes, *Nano Lett.*, 2011, **11**, 1928-1933.